

most suitable duration after administration for analysis of gene downregulation is recommended.

6. When the needle is correctly positioned into the left ventricle, bright red oxygenated blood influxes into the needle hub (13, 24). In this model, bone metastases developing in the jaws and/or legs of the mice are detected by non-invasive in vivo bioluminescence imaging.
7. For systemic administration of 200  $\mu$ l of the mixture, taking 20–30 s will enhance delivery efficacy.
8. In drug resistant tumors, sometimes in vivo bioluminescence imaging does not work well since the luciferin substrate and oligonucleotide mixture are not easily taken up by drug-resistant tumor cells (14).
9. Atelocollagen is a highly purified type I collagen that is modified to have low immunogenicity (Koken, Tokyo). Atelocollagen forms nanosize particles when it is mixed with synthetic miRNAs, via electrostatic binding. The nanoparticles are easily incorporated into cells by endocytosis. The atelocollagen/oligonucleotide complex showed high resistance to nucleases. Therefore, the complex is thought to be stable in vivo (12, 29).
10. It is possible to prepare luciferase-expressing cells with a virus vector system. To generate lentiviral-vector particles containing the luciferase gene, an HIV-1 gag-pol expression plasmid, an HIV-1 Rev expression plasmid and a VSV-G envelope protein expression plasmid were used to package the HIV-based expression vector. In brief, four plasmids were co-transfected into 293FT cells. Two days after transfection, the supernatants were cleared from the cellular debris by low-speed centrifugation (10 min, 1,000  $\times g$ ) and filtration through 0.45- $\mu$ m filters. Aliquots were stored at  $-80^{\circ}\text{C}$ .

---

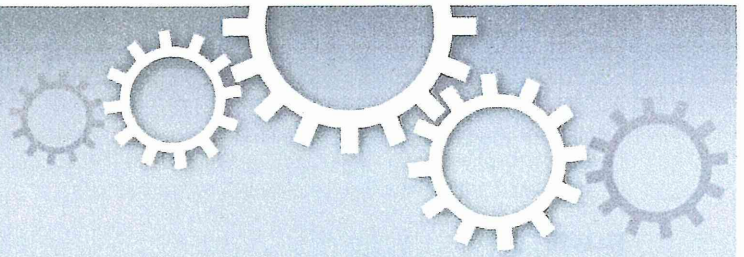
## Acknowledgements

This work was supported in part by a Grant-in-Aid for the Third-Term Comprehensive 10-Year Strategy for Cancer Control, a Grant-in-Aid for Scientific Research on Priority Areas Cancer from the Ministry of Education, Culture, Sports, Science and Technology, and the Program for Promotion of Fundamental Studies in Health Sciences of the National Institute of Biomedical Innovation (NiBio), and a Takeda Science Foundation.

## References

1. Bass, B.L. (2000) Double-stranded RNA as a template for gene silencing. *Cell* **101**, 235–238.
2. McManus, M.T. and Sharp, P.A. (2003) Gene silencing in mammals by small interfering RNAs. *Nat Rev Genet* **3**, 737–747.
3. Shankar, P., Manjunath, N., and Lieberman, J. (2005) The prospect of silencing disease using RNA interference. *JAMA* **293**, 1367–1373.
4. Leung, R.K., Whittaker, P.A. (2005) RNA interference: from gene silencing to gene-specific therapeutics. *Pharmacol Ther* **107**, 222–239.
5. Behlke, M.A. (2006) Progress towards in vivo use of siRNAs. *Mol Ther* **13**, 644–670.
6. Dykxhoorn, D.M., Palliser, D., and Lieberman, J. (2006) The silent treatment: siRNAs as small molecule drugs. *Gene Ther* **13**, 541–552.
7. Rayburn, E.R., Wang, H., and Zhang, R. (2006) Antisense-based cancer therapeutics: are we there yet? *Expert Opin Emerg Drugs* **11**, 337–352.
8. Hagan, J.P. and Croce, C.M. (2007) MicroRNAs in carcinogenesis. *Cytogenet Genome Res* **118**, 252–259.
9. Jiang, J., Gusev, Y., Aderca, I., Mettler, T.A., Nagorney, D.M., Brackett, D.J., Roberts, L.R., and Schmittgen, T.D. (2008) Association of microRNA expression in hepatocellular carcinomas with hepatitis infection, cirrhosis, and patient survival. *Clin Cancer Res* **14**, 419–427.
10. Bartel, D.P. (2004) MicroRNAs: genomics, biogenesis, mechanism, and function. *Cell* **116**, 281–297.
11. Osaki, M., Takeshita, F., and Ochiya, T. (2008) MicroRNA as biomarkers and therapeutic drugs in human cancer. *Biomarkers* **13**, 658–670.
12. Minakuchi, Y., Takeshita, F., Kosaka, N., Sasaki, H., Yamamoto, Y., Kouno, M., Honma, K., Nagahara, S., Hanai, K., Sano, A., Kato, T., Terada, M., and Ochiya, T. (2004) Atelocollagen-mediated synthetic small interfering RNA delivery for effective gene silencing in vitro and in vivo. *Nucleic Acids Res* **32**:e109.
13. Takeshita, F., Minakuchi, Y., Nagahara, S., Honma, K., Sasaki, H., Hirai, K., Teratani, T., Namatame, N., Yamamoto, Y., Hanai, K., Kato, T., Sano, A., and Ochiya, T. (2005) Efficient delivery of small interfering RNA to bone-metastatic tumors by using atelocollagen in vivo. *Proc Natl Acad Sci USA* **102**, 12177–12182.
14. Honma, K., Iwao-Koizumi, K., Takeshita, F., Yamamoto, Y., Yoshida, T., Nishio, K., Nagahara, S., Kato, K., and Ochiya, T. (2008) *RPN2* gene confers docetaxel resistance in breast cancer. *Nat Med* **14**, 939–948.
15. Takei, Y., Kadomatsu, K., Goto, T., and Muramatsu, T. (2006) Combinational antitumor effect of siRNA against midkine and paclitaxel on growth of human prostate cancer xenografts. *Cancer*, **107**, 864–873.
16. Vooijs, M., Jonkers, J., Lyons, S., and Berns, A. (2002) *Cancer Res* **62**, 1862–1867.
17. Hoffman, R.M. (1999) Orthotopic transplant mouse models with green fluorescent protein-expressing cancer cells to visualize metastasis and angiogenesis. *Cancer and Metastasis Reviews* **17**, 271–277.
18. Hoffman, R.M. (1999) Orthotopic metastatic mouse models for anticancer drug discovery and evaluation: a bridge to the clinic. *Invest New Drugs* **17**, 343–359.
19. Hoffman, R.M. (2002) In vivo imaging of metastatic cancer with fluorescent proteins. *Cell Death Differ* **9**, 786–789.
20. Hoffman, R.M. (2005) Orthotopic metastatic (MetaMouse) models for discovery and development of novel chemotherapy. *Methods Mol Med* **111**, 297–322.
21. Nakanishi, H., Ito, S., Mochizuki, Y., and Tatematsu, M. (2005) Evaluation of chemosensitivity of micrometastases with green fluorescent protein gene-tagged tumor models in mice. *Methods Mol Med* **111**, 351–362.
22. Hennig, R., Ventura, J., Segersverd, R., Ward, E., Ding, X.Z., Rao, S.M., Jovanovic, B.D., Iwamura, T., Talamonti, M.S., Bell, R.H. Jr, and Adrian, T.E. (2005) LY293111 improves efficacy of gemcitabine therapy on pancreatic cancer in a fluorescent orthotopic model in athymic mice. *Neoplasia* **7**, 417–425.
23. Contag, P.R., Olomu, I.N., Stevenson, D.K., and Contag, C.H. (1998) Bioluminescent indicators in living mammals. *Nat Med* **4**, 245–247.
24. Rehemtulla, A., Stegman, L.D., Cardozo, S.J., Gupta, S., Hall, D.E., Contag, C.H., and Ross, B.D. (2000) Rapid and quantitative assessment of cancer treatment response using in vivo bioluminescence imaging. *Neoplasia* **2**, 491–495.
25. Jenkins, DE, Oei, Y, Hornig, YS, Yu, S.F., Dusich, J., Purchio, T., and Contag, P.R. (2003) Bioluminescent imaging (BLI) to improve and refine traditional murine models of tumor growth and metastasis. *Clin Exp Metastasis* **20**, 733–744.

26. Vooijs, M., Jonkers, J., Lyons, S., and Bernes, A. (2002) Noninvasive imaging of spontaneous retinoblastoma pathway-dependent tumors in mice. *Cancer Res* **62**, 1862–1867.
27. Lyons, S.K. (2005) Advances in imaging mouse tumor models in vivo. *J Pathol* **205**, 194–205.
28. Laurie, N.A., Gray, J.K., Zhang, J., Leggas, M., Relling, M., Egorin, M., Stewart, C., and Dyer, M.A. (2005) Topotecan combination chemotherapy in two new rodent models of retinoblastoma. *Clin Cancer Res* **11**, 7569–7578.
29. Takeshita, F., Bader, A.G., Osaki, M., Takahashi, R., Yamamoto, Y., Kosaka, N., Kawamata, M., Kelnar, K., Brown, D., and Ochiya, T. (2010) Systemic delivery of miR-16 for RNAi therapy in prostate cancer. *Mol Ther* **18**, 181–187.



# Two distinct knockout approaches highlight a critical role for p53 in rat development

Masaki Kawamata & Takahiro Ochiya

Division of Molecular and Cellular Medicine, National Cancer Center Research Institute, 1-1, Tsukiji, 5-chome, Chuo-ku, Tokyo 104-0045, Japan.

SUBJECT AREAS:

PLURIPOTENCY

EMBRYONIC STEM CELLS

CANCER MODELS

MECHANISMS OF DISEASE

Received

17 July 2012

Accepted

29 October 2012

Published

10 December 2012

Correspondence and requests for materials should be addressed to T.O. (tochiya@ncc.go.jp)

Gene targeting in embryonic stem cells (ESCs) has become the principal technology for generating knockout models. Although numerous studies have predicted that the disruption of *p53* leads to increased developmental anomalies and malignancies, most *p53* knockout mice develop normally. Therefore, the role of *p53* in animal development was examined using rat knockout models. Conventionally generated homozygous KO males developed normally, whereas females rarely survived due to neural tube defects. Mutant chimeras generated via blastocyst injection with *p53*-null ESCs exhibited high rates of embryonic lethality in both sexes. This phenotype could be observed in one month by the use of zinc-finger nucleases. The *p53*-null ESCs were resistant to apoptosis and differentiation, and exhibited severe chromosome instabilities in the chimera-contributed cells, suggesting an essential role for *p53* in maintaining ESC quality and genomic integrity. These results demonstrate that *p53* functions as a guardian of embryogenesis in the rats.

Over the past two decades, knockout (KO) technology in mice has helped to clarify the physiological function of a large number of genes. However, unexpected phenotypes have been observed in some cases, making it difficult to understand the role of the deleted gene, or to translate that data to the phenotypes of human diseases caused by mutations in such genes. Thus, gene-targeting techniques for other animals, such as rats, have long been sought. Many strategies for manipulating rat genes to generate loss-of-function models have been adapted from the mouse genetic toolbox, including conventional transgenesis by pronuclear injection<sup>1</sup>, RNA interference<sup>2</sup>, N-ethyl-N-nitrosourea (ENU) mutagenesis<sup>3,4</sup>, and transposon mutagenesis<sup>5-7</sup>. KO rats have been produced using Zinc-finger nuclease (ZFN) technology<sup>8,9</sup>, and, most recently, germline-competent rat ESCs and rat induced pluripotent stem cells (iPSCs) have been established by the addition of cell-signaling inhibitors to the culture medium<sup>10-13</sup>, making it possible to generate both transgenic (Tg)<sup>12,14</sup> and KO rats<sup>15</sup>.

The tumor suppressor gene *p53* is a good example of a gene whose function in mouse development requires further scrutiny. Donehower et al. first reported normal Mendelian ratios and postnatal development in *p53* homozygous KO mice<sup>16</sup>. However, two other groups later showed that a fraction of homozygous KO females had fatal embryonic exencephaly, a defect in neural tube closure that results in an overgrowth of neural tissue in the midbrain region<sup>17,18</sup>. Such results indicate that, at least in some cases, *p53* influences development in females<sup>19</sup>. In the case of *p53* homozygous KO rats, neural tube defects (NTDs) in females were not found but increased susceptibility to tumor development was reported<sup>15,20,21</sup>.

*p53* has been shown to regulate not only cell cycle arrest, apoptosis, and DNA repair in many types of cells<sup>22</sup>, but also stemness, by suppressing *Nanog* expression in ESCs<sup>23</sup>. Considering these observations, malignant transformations may occur in *p53*-null ESCs and chimera development may be hindered. However, chimeric mutant mice have been successfully generated via the injection of blastocysts with iPSCs derived from *p53*-null mouse embryonic fibroblasts (MEFs), and germline transmission of the *p53*-null cells was also accomplished<sup>24,25</sup>. The properties of rat ESCs differ from those of mouse ESCs in that rat ESCs cannot be cultured in mouse ESC culture conditions due to their high sensitivity to differentiation signals<sup>26</sup>. Thus, an approach using *p53*-null rat ESCs might reveal new insights into the function of *p53* in regulating stemness and animal development.

We previously generated *Oct4*-Venus Tg rats, and established *Oct4*-Venus ESC lines in which *Oct4* expression can be monitored by green fluorescence<sup>12,27</sup>. Here, both conventionally KO and mutant chimeras rats were generated using *p53*-null *Oct4*-Venus ESCs, and their development was investigated. Moreover, an efficient

method for a rapid generation of mutant chimeras was developed using ZFN-mediated gene targeting in rat ESCs. Using this method, developmental phenotypes can be observed within 1 month.

## Results

**Conventionally generated  $p53^{-/-}$  females reveal the cause of NTDs.**  $p53$  homozygous KO rats were generated via germline transmission of heterozygous  $p53^{+/C}$  ESCs (Fig. 1a,b,e). The details are described in the *Materials and Methods*. The Mendelian ratios in weaned rats produced from heterozygous intercrosses were investigated (Fig. 2a). The frequency of homozygous  $p53^{C/C}$  rats was 16.9%, less than the anticipated value of 25% (Table 1). Moreover, only one  $p53^{C/C}$  female developed normally, frequency = 0.70%, significantly

less than 16.2%  $p53^{C/C}$  males. These results suggest that most of the  $p53^{C/C}$  females either do not survive gestation, or die after birth but prior to weaning. To investigate the developmental dysfunctions in  $p53^{C/C}$  females, litters from heterozygous intercrosses were examined at embryonic day 16.0 (E16.0) to E18.0. Eleven  $p53^{C/C}$  female embryos (12.8%, 11/86) were recovered at this stage; six (57%, 6/11) exhibited exencephaly (Table 1) and two of these also exhibited spina bifida (Fig. 2b). Although these two abnormalities are the most prevalent NTDs, spina bifida in  $p53$  mutant mice has only been reported in one study<sup>28</sup>. Exencephaly was only found in the female embryos, consistent with previous observations of a higher incidence of NTDs in human females and in numerous mouse models<sup>29</sup>. Expression of SOX2, a marker for primordial neuronal cells

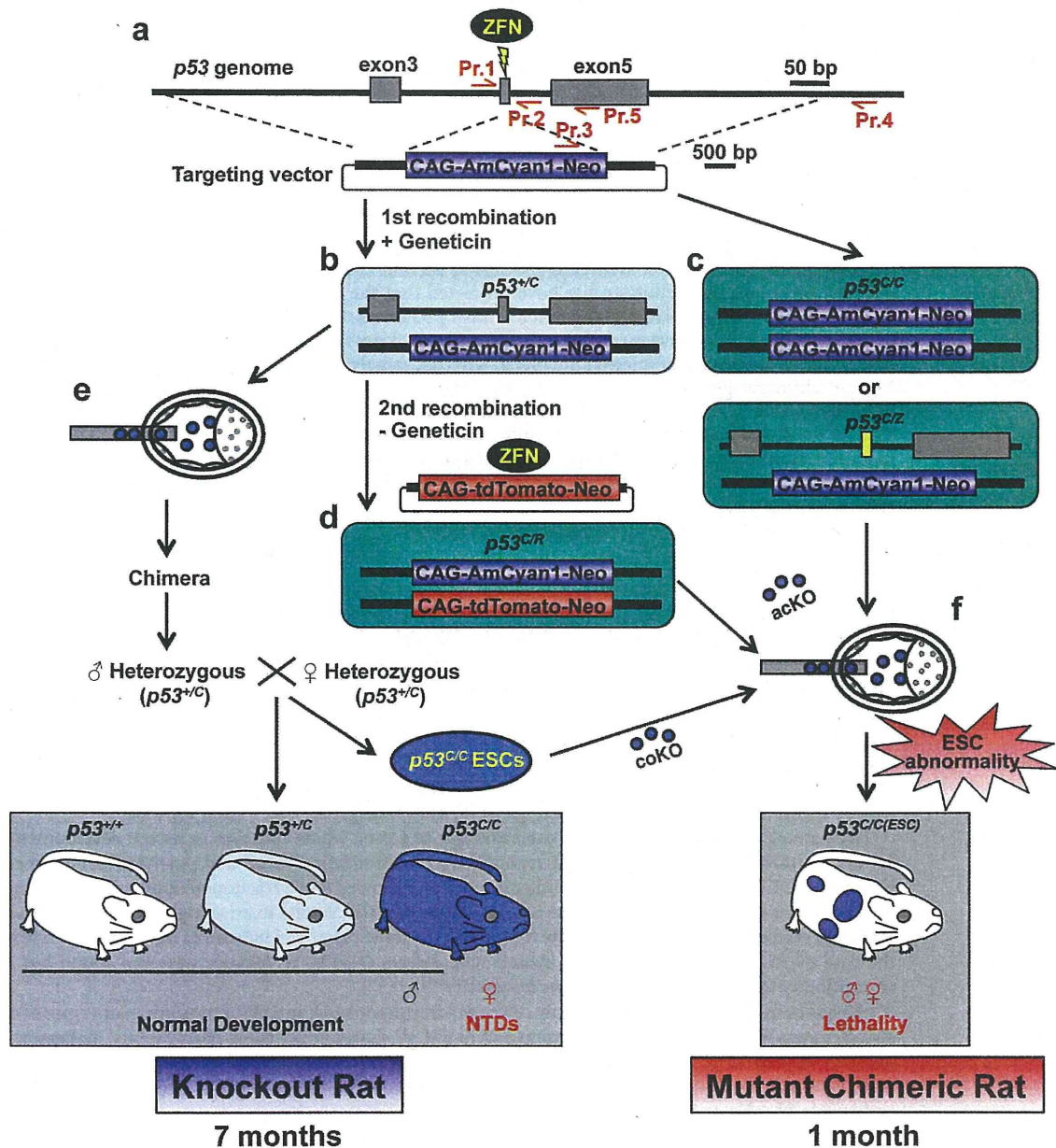


**Figure 1 | Schematic representation of  $p53$  KO strategy in rats.** (a–d) Both mono- (b) and bi-allelic (c) or 2ndary (d) homologous recombination are induced by ZFN. (e, f) Heterozygous or homozygous ESC-injection leads to the generation of conventionally generated KO model (e) or ESC-based mutant chimeric models (f), respectively. A yellow box indicates a frame shift mutation induced by ZFNs. Pr., Primer. coKO, congenital KO. acKO, acquired KO.


**Table 1 | The *p53* Genotypes of Adult and Embryonic Rats**

Genotype	<i>p53</i> <sup>+/+</sup>	<i>p53</i> <sup>+/-</sup>	<i>p53</i> <sup>C/C</sup>	<i>p53</i> <sup>C/C</sup> Exencephaly
Adults	41 (28.9%)	77 (54.2%)	24 (16.9%)	0
Male	18 (12.7%)	42 (29.6%)	23 (16.2%)	0
Female	23 (16.2%)	35 (24.6%)	1 (0.70%)	0
Embryos	21 (24.4%)	48 (55.8%)	17 (19.8%)	6
Male	11 (12.8%)	22 (25.6%)	6 (7.0%)	0
Female	10 (11.6%)	26 (30.2%)	11 (12.8%)	6 (54.5%) <sup>a</sup>

<sup>a</sup>Of the 11 *p53*<sup>C/C</sup> female embryos, six exhibited exencephaly.

expressed in the embryonic neural plate<sup>30</sup>, was detected on the surface of the brain and in areas of spina bifida (Fig. 2d, arrowheads), confirming that neural tube closure had failed. Compared to a *p53*<sup>+/-</sup> embryo (Fig. 2e, right), the aberrant ventricular zone (VZ) structure in the brain of a *p53*<sup>C/C</sup> exencephalic embryo was revealed by the localization of SOX2 (Fig. 2d left, arrows), which is expressed in the neuroendothelial stem cells of the VZ<sup>31</sup>. In this embryo, *Oct4*-Venus expressing cells were aberrantly located in the exencephalic region (Fig. 2b, green square, and 2c).

**Embryonic lethality in a mutant chimeric model.** ZFNs can create site-specific double-strand breaks, which are repaired via non-

homologous end joining, resulting in frame-shift mutations by the arbitrary addition or deletion of base pairs. Cotransfection of ZFNs with targeting vectors enhances homologous recombination, not only in human pluripotent cells<sup>32,33</sup>, but also in one-cell embryos, leading to the direct generation of knock-in mice<sup>34</sup> and rats<sup>35</sup>. In the present work, ZFNs were used to produce homozygous mutant ESC lines by a single recombination step (Fig. 1c). Using this approach, 1 of 46 (2.2%) clones harbored dual knock-in alleles (*p53*<sup>C/C</sup>), while 7 of 46 (15%) clones possessed both knock-in and frame shift mutant alleles (*p53*<sup>C/Z</sup>). In a 2nd-step recombination, homozygous clones were also produced from a *p53*<sup>+/-</sup> ESC clone based on the same strategy using both ZFNs and a targeting vector expressing red fluorescence (Fig. 1b,d). A successful homologous recombination was achieved in 3 of 8 clones (38%, *p53*<sup>C/R</sup>; Supplementary Fig. S2c). These ESC lines were called acquired KO (acKO) ESCs (Fig. 1c). The contribution of *p53*<sup>-/-</sup> (*p53*<sup>C/C</sup>, *p53*<sup>C/Z</sup>, or *p53*<sup>C/R</sup>) ESCs to rats, which are called *p53*<sup>-/- (ESC)</sup> rats, was examined, and the timeline for the rapid generation of the mutant chimeras is shown schematically (Fig. 3a,b). Microinjection of *p53*<sup>-/-</sup> ESCs into blastocysts led to the delivery of only a few pups ( $0.4 \pm 0.2$  per foster mother,  $n=5$ , 4 cell lines). This number ( $0.4 \pm 0.2$ /foster mother) was significantly smaller than the number of pups delivered following injection of *p53*<sup>+/+</sup> ESCs into blastocysts ( $4.0 \pm 1.1$  per foster mother,  $n=5$ , 3 cell lines,  $P<0.05$ ) or *p53*<sup>+/-</sup> (*p53*<sup>+/-</sup>) ESCs ( $5.1 \pm 1.1$  per foster mother,  $n=9$ , 4 cell lines,  $P<0.05$ ) (Fig. 3c). The

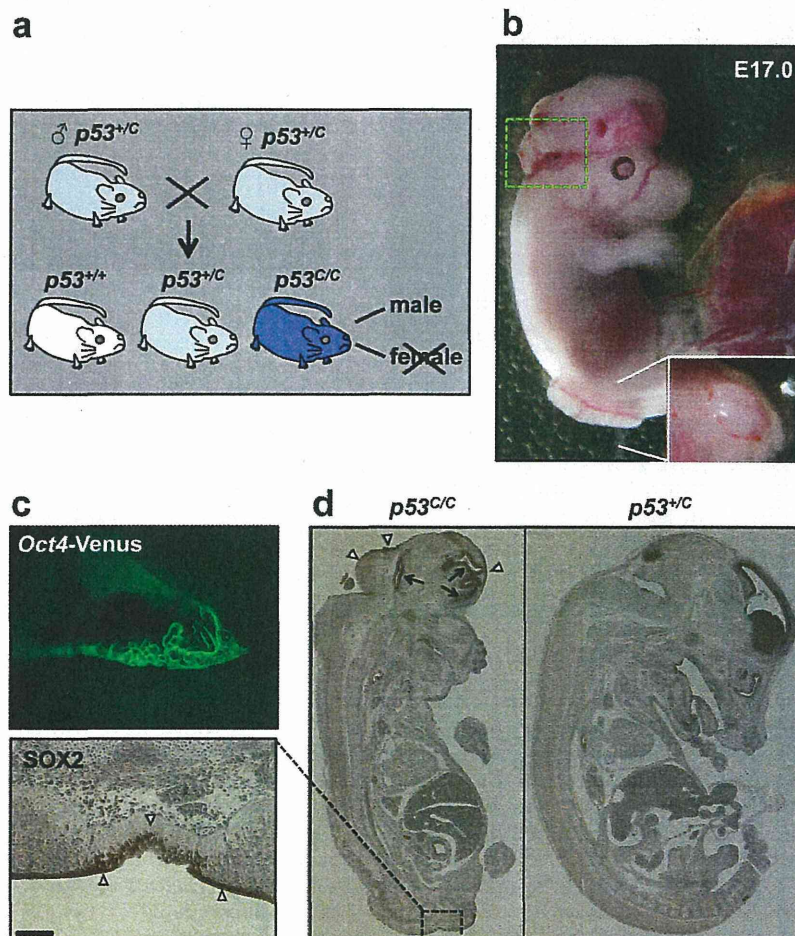


**Figure 2 | Phenotypes in conventionally generated *p53* homozygous rats.** (a) Schematic representation of heterozygous intercrosses indicates a loss of adult female. (b) An embryo at day 17.0 of gestation (E17.0) displaying exencephaly and spina bifida. A dotted green square indicates (c). (c) Fluorescence image of the area inside the dotted green square in (b). *Oct4*-Venus fluorescence is observed in the exencephalic region. (d) IHC staining for SOX2 identifies positive cells in the ventricular zone (arrows) and surface (arrowheads) of both brain and spina bifida (magnified image, scale bar = 100  $\mu$ m).

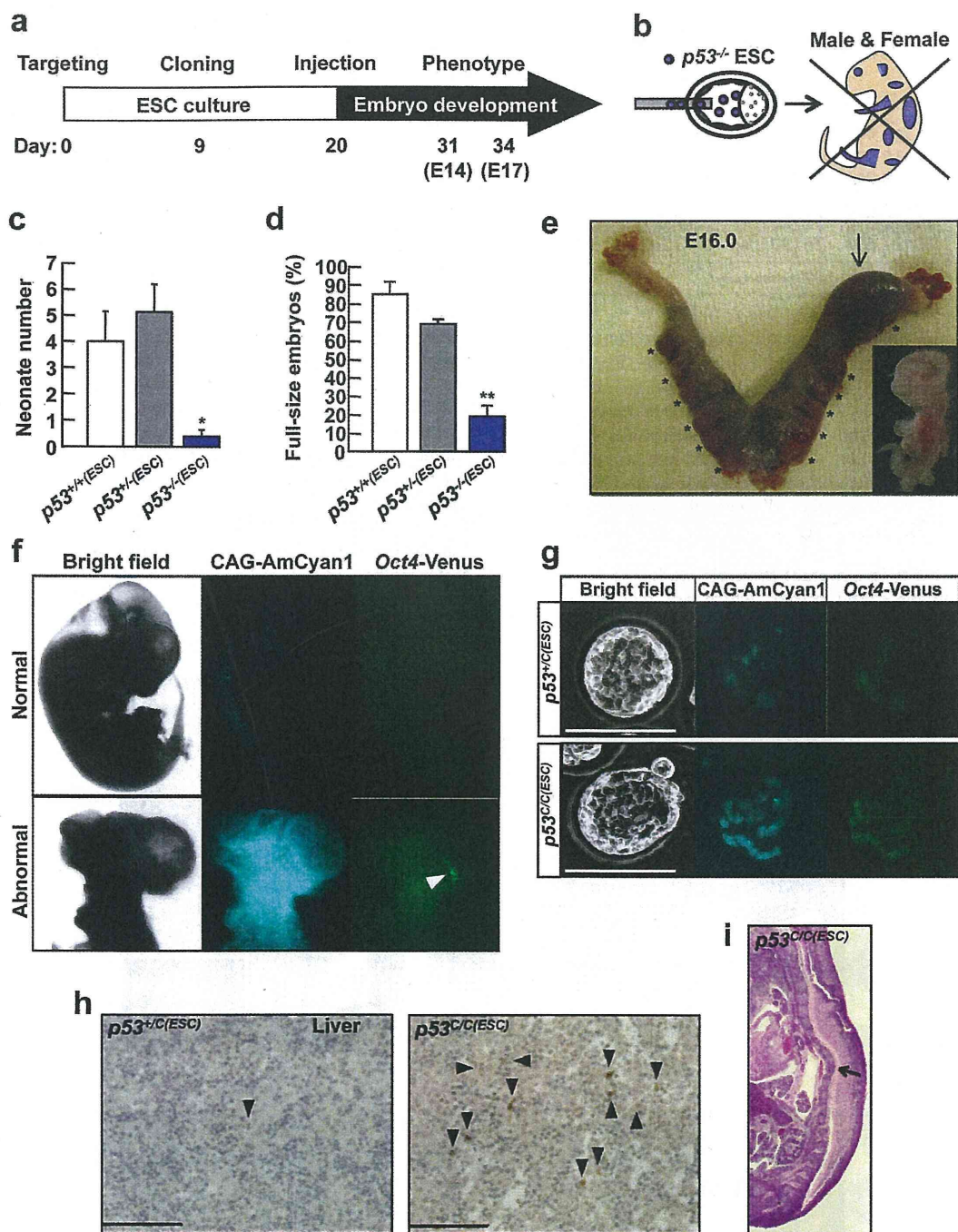


**Figure 3 | Embryonic lethality in  $p53$  mutant chimeras.** (a) Time line for generating  $p53^{-/-}$ (ESC) chimeras and (b) Schematic representation to investigate phenotype during embryogenesis. (c) Number of neonates successfully delivered.  $p53^{+/+}$  (n=5, 3 cell lines),  $p53^{+/-}$  (n=9, 4 cell lines) or  $p53^{-/-}$  (n=5, 4 cell lines) ESCs were injected into wild-type blastocysts. n, injection number. \*,  $P < 0.05$ ,  $p53^{-/-}$  vs.  $p53^{+/+}$  and  $p53^{+/-}$ . (d) The ratio of chimeric embryos with normal body size at E14.0 to E17.0.  $p53^{+/+}$  (n=4, 4 cell lines),  $p53^{+/-}$  (n=7, 4 cell lines) or  $p53^{-/-}$  (n=14, five cell lines) ESCs were injected into wild-type blastocysts. n, injection number. \*\*,  $P < 0.001$ ,  $p53^{-/-}$  vs.  $p53^{+/+}$  and  $p53^{+/-}$ . (e) Developmental dysfunction in chimeric embryos injected with  $p53^{C/R2}$  ESCs at E16.0. An arrow indicates a chimera with growth retardation (inset). Asterisks indicate fetal absorption. (f) Correlation between developmental dysfunction and ESC contribution.  $p53^{C/ESC}$  ESCs expressing AmCyan1 contribute to chimeric embryos at E14.0. An arrowhead indicates an ectopic expression of Oct4-Venus. (g)  $p53^{C/R4}$  ESC proliferation in blastocyst. Twelve ESCs were injected into blastocyst, followed by incubation overnight in YPAC medium. (h) Immunohistochemistry using Cleaved-Caspase3 antibody in liver of  $p53^{+/+}$ (ESC) or  $p53^{C/ESC}$  chimera. Arrowheads indicate the apoptotic cells. (i) Spinal curvature (an arrow) in  $p53^{C/ESC}$  chimera. All scale bars = 100  $\mu$ m.

newborns derived from  $p53^{-/-}$  ESC-injections did not exhibit a brown coat-color, indicating that they were not chimeras. Because these results suggest that the development of  $p53^{-/-}$ (ESC) embryos was

defective, fetal development at stages E14.0 to E17.0 was examined. Approximately 80% of the  $p53^{-/-}$ (ESC) embryos (n=14, 5 cell lines, Fig. 3d) showed abnormal development resulting in complete



resorption (Fig. 3e, asterisks) or growth retardation (Fig. 3e, an arrow and inset). A large number of  $p53^{-/-}$  ESC-derived cells were detected in these embryos (Fig. 3f, lower). However, the remaining  $p53^{-/-}$  (ESC) embryos (30/189 embryos:  $20.0 \pm 5.6\%$ ) developed a normal body size (Fig. 3f, upper and Supplementary Table S1). The number of normal embryos ( $20.0 \pm 5.6\%$ ) was significantly lower than that of  $p53^{+/+}$  (ESC) embryos (53/63 embryos:  $85.1 \pm 5.8\%$ ,  $n=4$ , 4 cell lines,  $P<0.01$ ) or  $p53^{+/-}$  (ESC) embryos (44/64 embryos:  $69.0 \pm 2.2\%$ ,  $n=7$ , 4 cell lines,  $P<0.01$ ) (Fig. 3d). Among the normal-sized  $p53^{-/-}$  (ESC) embryos, 26 of 30 ( $87.8 \pm 9.7\%$ ,  $n=10$ , 5 cell lines) embryos were chimeras, whereas 22 of 26 displayed a relatively lower contribution of the mutant cells. Although the number of  $p53^{+/-}$  (ESC) chimera (30/44 embryos,  $66.9 \pm 6.6\%$ ,  $n=7$ , 4 cell lines) was similar to that of  $p53^{-/-}$  (ESC) chimera (14/14), the  $p53^{+/-}$  (ESC) chimera developed normally (Fig. 3c, d). The number of  $p53^{+/+}$  (ESC) chimera (17/53 embryos,  $36.0 \pm 10.2\%$ ,  $n=4$ , 4 cell lines) was significantly smaller than that of either  $p53^{+/-}$  (ESC) ( $P=0.044$ ) or  $p53^{-/-}$  (ESC) ( $P=0.0081$ ) chimera. These results suggest that  $p53$  mutation enhances the chimeric contribution of ESCs and the high contribution of  $p53$ -null ESCs induces embryonic lethality.

To address the mechanisms by which  $p53^{-/-}$  ESCs result in embryonic lethality, the behavior of  $p53^{-/-}$  ESCs was followed in blastocysts incubated *in vitro*. Blastocysts were injected with 12 ESCs and incubated over night. Although  $p53^{+/+}$  ESCs remained

in the blastocysts, the number decreased to  $4.0 \pm 0.89$  cells (Fig. 3g, upper,  $n=5$ ). In contrast, a significantly larger number of  $p53^{C/R4}$  ESCs ( $13.7 \pm 1.2$  cells,  $n=7$ ,  $P<0.0001$ ) were detected (Fig. 3g, lower), indicating proliferation of the  $p53$ -null ESCs in the blastocysts. The excess proliferation may lead to a high ESC contribution, resulting in the developmental abnormalities that led to resorption of the fetuses. In fact, several of the  $p53^{C/C(ESC)}$  chimeras with normal body size displayed increased number of apoptotic cells in the liver (Fig. 3h, arrowheads) and one chimera exhibited an abnormal spinal curvature (Fig. 3i, an arrow). Embryos such as these may die and undergo resorption before birth, resulting in the significant loss of neonates as shown in Figure 3d.

**Morphology and global gene expression profile in  $p53^{-/-}$  ESCs.** The properties of  $p53^{-/-}$  ESCs were examined. Venus-negative differentiated cells (Fig. 4a, left, arrowheads) survived the processes of cloning and passing  $p53^{-/-}$  Venus-positive ESCs (Fig. 4a, left, arrows), indicating that  $p53^{-/-}$  differentiated cells escaped from apoptosis. Rat ESC colonies adopt a dome-shaped morphology and tend to detach from culture dishes coated with MEFs<sup>12,15</sup>. The  $p53^{-/-}$  domed colonies were detached by pipetting and the cells were passaged after dissociation, leading to successful propagation of dome-shaped colonies; no differentiated cells were detected. (Fig. 4a, right, arrows). The morphology of the  $p53^{-/-}$  lines was

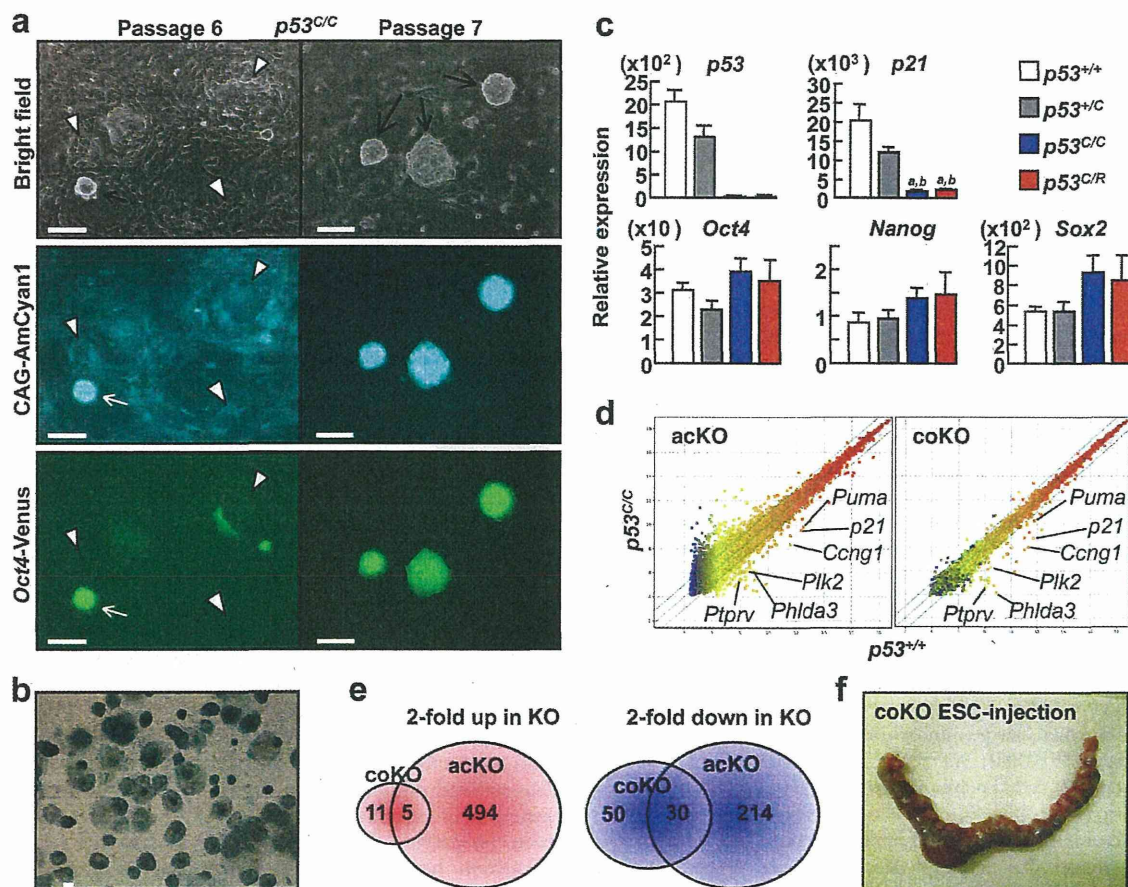


**Figure 4 | Characteristics of  $p53$ -null ESCs.** (a) A  $p53^{C/C}$  ESC clone is shown. Arrows indicate pluripotent colonies. Arrowheads indicate differentiated cells. (b) ALP staining in  $p53^{C/C}$  ESCs. (c) q-PCR analysis in  $p53$  mutant ESCs. Transcript levels were normalized to *Gapdh* levels. Data are the mean  $\pm$  SD of one biological sample assayed in four independent experiments. *a*,  $P<0.05$  versus  $p53^{+/+}$ ; *b*,  $P<0.005$  versus  $p53^{+/-}$ . (d) Scatter plots of global gene expression microarrays comparing  $p53^{+/+}$  and  $p53^{C/C}$  ESCs of an acKO (left) or coKO (right) line. The green lines delineate the boundaries of a 2-fold difference in gene expression levels. (e) Venn diagrams of the intersection between genes highly (left) or lowly (right) expressed in the coKO versus the acKO in  $p53^{C/C}$  ESCs. (f) Developmental dysfunction in chimeric embryos injected with  $p53^{C/C2}$  coKO ESCs at E16.0. All scale bars = 100  $\mu$ m.



indistinguishable from that of  $p53^{+/-}$  or  $p53^{+/+}$  cells (Supplementary Fig. S3). The  $p53^{CC}$  ESCs were positive for alkaline phosphatase (ALP) activity (Fig. 4b).

The expression levels of ESC marker genes, such as *Oct4*, *Nanog* and *Sox2*, were similar in  $p53^{CC}$  and  $p53^{CR}$  ESCs compared to  $p53^{+/+}$  or  $p53^{+/C}$  cells, whereas loss of *p53* mRNA and parallel reduction in the mRNA level of the *p53* target gene *p21* were confirmed in mutant ESC lines (Fig. 4c). The ESC line produced by acquired gene targeting in wild-type ESCs ('acKO' ESCs) and a congenital KO ESC line derived from heterozygous intercrosses (named coKO) were analyzed to determine whether some compensatory effect occurred in the coKO line. A microarray analysis showed that the coKO line had less divergent expression compared to the acKO line (acKO vs. coKO: 494 vs. 11 genes upregulated and 214 vs. 50 genes downregulated, Fig. 4e). Venn diagrams showing the overlap in genes identified in the two KO ESC datasets identified only five upregulated and 30 downregulated genes (Fig. 4e, and see Supplementary Table S2). Many of the downregulated genes in the  $p53^{CC}$  ESCs were direct targets of *p53*, such as *Puma*, *p21*, *Ccng1*, *Plk2*, *Phlda3*, and *Ptprv* (Fig. 4d), whereas no genes for pluripotency or stemness were identified.

Chimera generation was used to investigate whether microinjection with these coKO ESCs could rescue mutant chimera development. Male ESC lines were also examined because homozygous males showed normal development. However, microinjection of both female cell lines ( $n=4$ , 2 cell lines) and male coKO ESC cell lines ( $n=7$ , 3 cell lines) produced chimeras in which embryogenesis failed, similar to the acKO chimeras (Fig. 4f and Supplementary Table S1). The fraction of full-sized embryos (15/68 embryos:  $23.1 \pm 4.0\%$ ,  $n=9$ , 5 cell lines) was similar to that of acKO chimeras (30/189 embryos:  $20.0 \pm 5.6\%$ ,  $n=14$ , 5 cell lines). These results indicate that lethality in mutant chimeras is due to abnormality of  $p53^{-/-}$  ESCs.

#### $p53^{-/-}$ ESCs are resistant to apoptosis and differentiation.

To investigate susceptibility to apoptosis, flow cytometry to detect surface exposure of Annexin V was performed in ESCs under routine culture conditions using YPAC medium [Y, Y-27632 (ROCK inhibitor); P, PD0325901 (MEK inhibitor); A, A-83-01 (TGF- $\beta$  inhibitor); C, CHIR99021 (GSK3 inhibitor)]<sup>12</sup>. A control treatment with G418 caused an increase in Annexin V-positive apoptotic cells whereas each of the *p53* genotype ESCs exhibited small population of the apoptotic cells ( $p53^{+/+}$ ,  $11.0 \pm 0.25\%$ ;  $p53^{+/C}$ ,  $14.0 \pm 0.30\%$ ;  $p53^{CC}$ ,  $11.0 \pm 0.49\%$ ) (Fig. 5a). Assays for colony formation and embryoid body (EB) formation were performed under differentiation culture conditions to examine the behavior of the mutant ESCs. There was no genotype-dependent difference in the numbers of undifferentiated or differentiated colonies under conditions using YPAC medium and MEFs (Fig. 5b). Under culture conditions using Y media and MEFs (inhibitors P, A and C were absent, Fig. 5c), almost no  $p53^{+/+}$  undifferentiated colonies formed ( $1.7 \pm 0.9$  colonies) but some  $p53^{+/C}$  colonies were observed ( $13.0 \pm 2.1$  colonies,  $P<0.01$ ). Few differentiated colonies of either genotype were formed. In contrast,  $p53^{CC}$  cells formed a large number of both undifferentiated ( $56.0 \pm 2.6$  colonies,  $P<0.0001$  vs.  $p53^{+/+}$ ;  $P<0.001$  vs.  $p53^{+/C}$ ) and differentiated ( $26.3 \pm 1.5$  colonies,  $P<0.0001$  vs.  $p53^{+/+}$ ;  $P<0.0001$  vs.  $p53^{+/C}$ ) colonies (Fig. 5c). These results suggest that  $p53^{-/-}$  ESCs strongly maintain both undifferentiated state and self-renewal capacities while the differentiated cells are protected from apoptosis, consistent with the results shown in Figure 3a. Next, colony formation was assessed under culture conditions in which ESCs weakly attach to un-coated culture dishes in the absence of MEFs. Although undifferentiated colony formation was rare in both  $p53^{+/+}$  ( $11.3 \pm 3.5$ ) and  $p53^{+/C}$  ( $2.0 \pm 1.2$ ) ESCs, a large number of  $p53^{CC}$  ESCs formed colonies ( $96.7 \pm 2.8$  colonies,  $P<0.0001$  vs.  $p53^{+/+}$ ;  $P<0.0001$  vs.  $p53^{+/C}$ ; Fig. 4d). In the un-coated dishes in

the absence of MEFs, differentiated colonies were rarely formed from any ESC genotype. Thus, the  $p53^{-/-}$  ESCs might have an increased capacity to adhere tightly to the culture dish and/or proliferate without the support of feeder cells.

When EB formation was examined,  $p53^{+/+}$  EBs formed by day 3 underwent apoptosis over time in culture, resulting in few EBs remaining by day 7 relative to day 3. In addition, Venus fluorescence was completely lost in these cells (Fig. 5e, left). In contrast,  $p53^{CC}$  EBs were large in size and number, and maintained Venus fluorescence (Fig. 5e, right). The number of cells in  $p53^{CC}$  EBs ( $3.25 \times 10^5$ ) was significantly larger than cell number in  $p53^{+/+}$  EBs ( $1.00 \times 10^3$ ,  $P<0.01$ ) or  $p53^{+/C}$  EBs ( $2.47 \times 10^4$ ,  $P<0.01$ ). Moreover, these data indicate that  $p53^{CC}$  EBs actively proliferated because the cell number increased from  $2.5 \times 10^5$  at day 0 to  $3.25 \times 10^5$  by day 7 (Fig. 5f). This result suggests that  $p53^{CC}$  cells are able to proliferate even in the absence of cell attachment.  $p53^{+/C}$  EBs showed an intermediate phenotype with significant differences from the other genotypes ( $P<0.01$  vs.  $p53^{+/+}$ ,  $P<0.01$  vs.  $p53^{CC}$ ).

**Chromosomal instability in  $p53^{-/-}$  cells.** Next, karyotype analysis was performed in  $p53^{-/-}$  cells. Although  $p53^{+/C}$  ESCs maintained a normal karyotype 42,XX,[20], one  $p53^{CR2}$  ESC clone exhibited abnormal karyotype 42,XX,add(15)(q22)[20] (Fig. 6a, red square and arrow). Moreover, once the  $p53^{CR2}$  ESC clone differentiated under EB forming culture conditions for two weeks (Fig. 6b), an additional chromosomal aberration, 41,X,-X,add(15)(q22)[20], was found in all cells analyzed (Fig. 6a, blue square). In a  $p53^{CC1}$  ESC clone, ESCs did not have an abnormal karyotype (42,XX[20]). However, cells derived from the  $p53^{CC1(ESC)}$  chimera in E14.0 rats displayed various chromosomal aberrations, such as 42,XX,add(1)(q52)[1], 42,XX,add(3)(p12)[1], 43,XX,+16[1] or 42,X,-X,+mar[1]. In cell cultures,  $p53^{+/+}$  cells derived from a recipient blastocyst were eliminated, resulting in occupation by  $p53^{CC1}$  cells with AmCyan1 expression (Fig. 6c).

These findings demonstrate that  $p53^{-/-}$  ESCs exhibit several features of abnormalities, such as blockage of differentiation, induction of chromosomal instability, and escape from apoptosis, which are facilitated when the cells differentiate. Thus, *p53* is indispensable for embryonic development in the mutant chimeric models (Fig. 1f) but dispensable in the homozygous models due to bypassing an ESC state (Fig. 1e).

## Discussion

Here, two distinct strategies were used to generate *p53* KO rats: conventionally generated homozygous KO and ESC-based mutant chimeras. In the homozygous KO rats, NTDs such as exencephaly and spina bifida were observed. This is the first NTD model created in genetically modified rats. Previously, a 50% reduction in the number of females relative to males at weaning was observed in *p53* homozygous KO mice<sup>17</sup>. In contrast, in the present study, a 96% reduction in the number of *p53* homozygous KO female rats surviving to weaning relative to homozygous KO males was observed (Table 1). In rats, exencephaly occurred in a large fraction of the homozygous KO females (55%; Table 1), whereas only 8–16% of homozygous KO female mouse embryos exhibited exencephaly<sup>17,18</sup>. The survival ratio and spina bifida phenotype observed in these exencephalic rat embryos suggests that this species exhibits more severe phenotypes than mice. We hypothesize that rats are more sensitive to the stress of DNA damage than mice. Consistent with this observation, rat ESCs are more sensitive to differentiation signals than mouse ESCs, which is one reason why rat ESCs were not established until 2008. Mouse ESCs are very stable compared to other species. In mouse, successful chimera contribution and germline transmission using *p53*-null mouse iPSCs has been reported<sup>24,25</sup>. These results were unexpected, considering the vast amount of data regarding the effects of *p53* on cell cycle arrest, apoptosis, and DNA

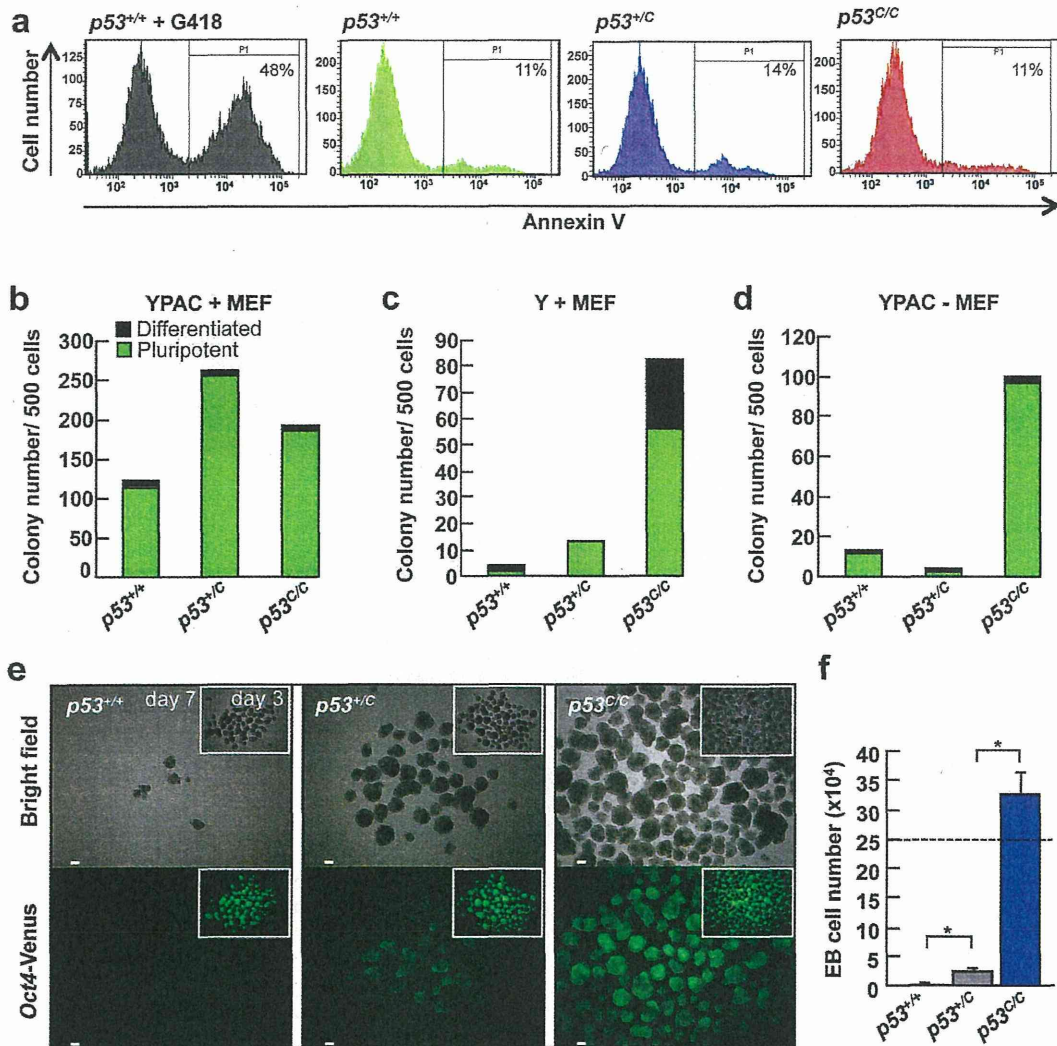


**Figure 5** | Colony and EB formation assays under differentiating conditions. (a) Flow cytometry analysis. Annexin V-Cy5 was used to detect apoptotic cells ( $n=3$ ). (b–d) Colony formation assay. Five hundred cells were cultured under normal conditions (YPAC+MEF; b), differentiation conditions (Y+MEF; c), or apoptosis-inducing conditions (YPAC-MEF; d). A green or black bar indicates pluripotent or differentiated colony number, respectively ( $n=3$  or 4). (e, f) EB formation assay. EBs were formed from  $2.5 \times 10^5$  cells (f, dotted line). Seven days after incubation without inhibitors, the cell number was counted (f,  $n=3$ ). Insets (e) indicate EBs at day 3. \*,  $P < 0.01$ . All scale bars = 100  $\mu\text{m}$ .

repair. In contrast, in the present study, mutant chimeras generated with rat ESCs demonstrated a clear phenotype of embryonic lethality, consistent with the data presented here showing the down-regulation of *p53* target genes, inhibition of apoptosis and differentiation, and increase in chromosomal instability in *p53*-null rat ESCs or ESC-derived cells.

The rat is considered to be a better model than the mouse for many complex disorders that are common in humans<sup>36</sup> and is currently the primary animal model in many preclinical tests, especially those related to cardiovascular disease, diabetes, breast cancer, chronic inflammatory diseases, and age-related diseases<sup>20</sup>. Genetically modified rats are valuable platforms for the study of human physiology and disease. For example, in comparison to transgenic mice, transgenic rat models of Huntington disease not only present a more typical adult patient pathology but are also more suitable for *in vivo* metabolic and structural imaging<sup>20,37</sup>. In addition, *Apc* knockout mice develop tumors primarily in the small intestine, whereas both humans and rats develop colon cancer as a result of the *Apc* mutation<sup>38</sup>. These observations support the inconsistent phenotype of *p53*

mutant chimeras between rats and mice, as shown in the present work, and suggest the importance of generating genetically modified rats to find novel gene functions.

In this study, the differences in the phenotypes of the *p53* homozygous and mutant chimeric rat models were striking. Secondary mutations are accumulated in the mutant ESCs under *in vitro* culture conditions and in the differentiating cells during embryogenesis (Fig. 6). These aberrant cells are resistant to apoptosis due to *p53* deficiency, which might lead to lethality of the mutant chimeras. These observations reflect the fact that a major *p53* function is to be the “guardian of the genome”. Thus, the mutant chimeric strategy may prove useful in identifying authentic and/or novel gene functions. Finally, the present study demonstrated that mutant chimeric models can be generated within one month, circumventing both the risks associated with producing successful germline transmission as well as the time frame required for breeding both chimeras and heterozygous animals. In the mutant chimeric method, double or triple gene knockouts can be generated in a few months. These new combination strategies using embryonic stem cells, the mutant